Biology Direct

RESEARCH

Open Access

The antipsychotic medications aripiprazole, brexpiprazole and cariprazine are off-target respiratory chain complex I inhibitors

Rachel E. Hardy[1], Injae Chung[2], Yizhou Yu[1], Samantha H. Y. Loh[1], Nobuhiro Morone[1], Clement Soleilhavoup[1], Marco Travaglio[1], Riccardo Serreli[2], Lia Panman[1], Kelvin Cain[1], Judy Hirst[2], Luis M. Martins[1*], Marion MacFarlane[1*] and Kenneth R. Pryde[1*]

Abstract

Antipsychotic drugs are the mainstay of treatment for schizophrenia and provide adjunct therapies for other prevalent psychiatric conditions, including bipolar disorder and major depressive disorder. However, they also induce debilitating extrapyramidal syndromes (EPS), such as Parkinsonism, in a significant minority of patients. The majority of antipsychotic drugs function as dopamine receptor antagonists in the brain while the most recent 'third'-generation, such as aripiprazole, act as partial agonists. Despite showing good clinical efficacy, these newer agents are still associated with EPS in ~ 5 to 15% of patients. However, it is not fully understood how these movement disorders develop. Here, we combine clinically-relevant drug concentrations with mutliscale model systems to show that aripiprazole and its primary active metabolite induce mitochondrial toxicity inducing robust declines in cellular ATP and viability. Aripiprazole, brexpiprazole and cariprazine were shown to directly inhibit respiratory complex I through its ubiquinone-binding channel. Importantly, all three drugs induced mitochondrial toxicity in primary embryonic mouse neurons, with greater bioenergetic inhibition in ventral midbrain neurons than forebrain neurons. Finally, chronic feeding with aripiprazole resulted in structural damage to mitochondria in the brain and thoracic muscle of adult *Drosophila melanogaster* consistent with locomotor dysfunction. Taken together, we show that antipsychotic drugs acting as partial dopamine receptor agonists exhibit off-target mitochondrial liabilities targeting complex I.

Introduction

Schizophrenia is a serious neurological disorder affecting 10–40 in 100,000 individuals [1]. Pharmacological alleviation and prevention of psychosis is the primary clinical goal. Hyper-active dopamine signalling in the mesolimbic dopaminergic circuit is proposed to contribute to the pathology of schizophrenia [2]. Therefore, antagonists of dopamine D2 and D3 receptors (D2R/D3R) represent a viable treatment approach [3]. First- and second-generation D2R/D3R antagonists (e.g. haloperidol and risperidone) are therapeutically effective but also cause dose-limiting, serious neurological adverse events in a substantial proportion of patients (~ 20 to 40%) [4]. They include severe extrapyramidal symptoms (EPS) such as

*Correspondence:
Luis M. Martins
lm795@mrc-tox.cam.ac.uk
Marion MacFarlane
mm2312@mrc-tox.cam.ac.uk
Kenneth R. Pryde
krp30@cantab.net
[1] MRC Toxicology Unit, University of Cambridge, Gleeson Building, Tennis Court Road, Cambridge CB2 1QR, UK
[2] MRC Mitochondrial Biology Unit, University of Cambridge, The Keith Peters Building, Cambridge Biomedical Campus, Hills Road, Cambridge CB2 0XY, UK

dystonia, akathisia, Parkinsonism, and tardive dyskinesia, which frequently lead to suspension of treatment [5–11]. The side-effects result from the on-target mechanism-of-action (MoA), which can suppress dopamine signalling to pathological levels and impair the nigrostriatal regulatory circuit that controls motor function. To reduce the incidence of neurological adverse events, third-generation antipsychotic drugs with a novel MoA have been developed. Specifically, aripiprazole (first approved for schizophrenia in the USA in 2002, with approximately 6 million prescriptions in 2017 [12]) functions as a partial D2R/D3R agonist and alleviates hyper-activation of dopaminergic circuits by competing for receptor binding with dopamine. It also prevents D2R/D3R hyper-activation during periods of excessive pre-synaptic dopamine release (as observed in the striatum of schizophrenic patients) [13, 14]. Pharmacologically, the partial agonists succeed because their slow k_{off} rates mean that they remain bound to the D2R/D3R—even when dopamine levels transiently spike to pathological levels [15].

Aripiprazole has been approved for an expanded number of indications in both adult and juvenile patient populations: for bipolar disorders (suppression of manic episodes), major-depressive disorder and autism [16–19]. Clinically, aripiprazole exhibits improved tolerability with a decreased frequency of neurological side effects (~5 to 15%) [20–22]. However, an unexpected minority of patients still experience severe movement disorders, both upon starting treatment and after prolonged treatment. In some instances, neurological dysfunction is irreversible following aripiprazole discontinuation [23, 24]. The molecular mechanisms driving neurotoxicity remain unclear, but these clinical observations could suggest that aripiprazole exhibits an underlying off-target effect that drives permanent neuronal damage in a minority of patients.

Mitochondria are essential for ATP production in neurons and integral to their function and homeostasis [25]. Mitochondrial dysfunction is broadly implicated in human neurodegeneration [26], affecting neurons that control movement. Specifically, mitochondrial activity is decreased in post-mortem brains of Parkinson's disease (PD) patients [27–29], mutations in proteins controlling mitochondrial homeostasis causes early-onset PD [30, 31], and treating animals with the mitochondrial respiratory-chain complex I inhibitors rotenone or MPP^+ recapitulates PD pathophysiology [32, 33]. More broadly, mitochondrial inhibition is an important off-target mechanism of drug-induced-toxicity, contributing to drug attrition in clinical trials as well as drug withdrawal following approval due to severe adverse events [34, 35].

The interactions between aripiprazole and mitochondria are not understood. Here, we investigated whether off-target mitochondrial toxicity could be an underlying cause of adverse motor side-effects in patients taking aripiprazole. Using a suite of cellular and cell-free biochemical assays, we demonstrate that aripiprazole and its primary active metabolite, dehydroaripiprazole, are off-target cytotoxic mitochondrial respiratory-chain inhibitors. Both compounds selectively inhibited respiratory-chain complex I, at patient-relevant concentrations, and we defined inhibition of the complex I ubiquinone-binding site (Q-site) as the molecular-initiating-event (MIE) driving toxicity. Feeding *Drosophila melanogaster* food supplemented with the complex I inhibitor aripiprazole induced mitochondrial ultrastructural abnormalities in the brain and thoracic muscle that were linked with the development of significant locomotor defects. Finally, we reveal that two further clinically-approved third-generation antipsychotics, brexpiprazole and cariprazine, also specifically inhibit the Q-site of complex I. These data demonstrate that aripiprazole, brexpiprazole and cariprazine share a common off-target mechanism that drives mitochondrial and cellular toxicity.

Results

Aripiprazole and its primary active metabolite are toxic to cells in a manner consistent with mitochondrial toxicity

To determine the propensity of individual antipsychotic drugs for off-target mitochondrial toxicity, we employed the glucose-to-galactose metabolic shift assay [36]. Briefly, galactose metabolism provides no net gain of ATP molecules from glycolysis, forcing the cell (particularly tumour cells that consume large amounts of glucose due to their Warburg phenotype) to rely on mitochondrial oxidative phosphorylation for ATP production. Thus, diverse mitochondrial toxicants can be uncovered using this model.

We treated human neuroblastoma cells (SH-SY5Y) cultured in glucose or galactose-containing media with 10 μM of each of 11 antipsychotic drugs from different classes for 18 h (Fig. 1A). Total cellular ATP levels were used as an endpoint to identify potential mitochondrial toxicants, with a selective reduction in galactose-conditioned cells as the criterion. Our screen showed that cellular ATP levels were selectively reduced in galactose-conditioned cells only by aripiprazole (Fig. 1A). Although chlorpromazine also induced a modest decline in cellular ATP levels, this was observed in both glucose and galactose-cultured cells. No effects were observed with iloperidone, lurasidone, haloperidol, risperidone, olanzapine, quetiapine, clozapine, zotepine or paliperidone. 2-Deoxyglucose (2-DG; a well-characterized inhibitor of glycolysis), piericidin A (a potent complex I inhibitor) and antimycin A (a potent complex III inhibitor) were used as positive controls.

Next, concentration-titrations were performed with aripiprazole and its primary active metabolite dehydroaripiprazole. Levels of dehydroaripiprazole in patient serum are ~ 40% of the parent compound [37]. Therefore, it was important to clarify whether the galactose-selective toxicity of aripiprazole was retained following metabolism. Both compounds induced dose-dependent declines in cellular ATP levels in galactose-conditioned SH-SY5Y cells after 18 h treatment (Fig. 1B). The IC_{50} values (concentrations required for 50% inhibition) for aripiprazole and dehydroaripiprazole were both 9 μM, with concentrations of 5 μM inducing modest declines (20–30%) in cellular ATP levels.

Further investigation demonstrated that both aripiprazole and dehydroaripiprazole promote cell death in a galactose-selective manner. Both compounds (5 μM) induced cell death after 18 h treatment, with a significant increase at 10 μM (~ 43% for aripiprazole and ~ 20% for dehydroaripiprazole) (Fig. 1C and Additional file 1: Fig. S1). Furthermore, clear reductions in cellular proliferation rate were observed in galactose-conditioned SH-SY5Y cells treated with 5 or 10 μM of each compound over an 86 h period (Fig. 1D and Additional file 1: Fig. S2). Therefore, we have identified aripiprazole and its primary pharmacologically active metabolite to be selectively toxic to SH-SY5Y cells cultured in galactose-medium: they diminish cellular ATP, viability and proliferative rate in a manner consistent with mitochondrial toxicity.

Aripiprazole and structurally-related antipsychotic drugs inhibit ubiquinone reduction by mitochondrial respiratory complex I

Next, we sought to determine the direct effects of aripiprazole and dehydroaripiprazole on mitochondrial bioenergetic function. Based on profound similarities in chemical substructure, we also investigated the more recently approved antipsychotic compounds brexpiprazole and cariprazine, as well as didesmethylcariprazine: a primary active metabolite of cariprazine [16].

Extracellular flux analysis was employed to assess the effects of the drugs on mitochondrial respiration. The assays were carried out in serum-free media to enable the effects to be assessed without any interference from drug-serum binding; aripiprazole and dehydroaripiprazole are known to be highly bound (> 99%) to plasma proteins in patients [38]. In experiments using foetal bovine serum to compare SH-SY5Y cells cultured in serum-supplemented or serum-free galactose-media, 10 μM aripiprazole or dehydroaripiprazole both induced greater declines in ATP levels in cells in serum-free media (Additional file 1: Fig. S3A), consistent with this fact.

The oxygen consumption rate (OCR), which depends on the function of the electron-transport chain (ETC), was measured in SH-SY5Y cells treated with varying concentrations of each drug (see Additional file 1: Fig. S3B for schematic of a standard mitochondrial respiration stress test). Importantly, we observed a significant decline in both basal and maximal OCR following a 4 h treatment with aripiprazole, dehydroaripiprazole, brexpiprazole or cariprazine, indicating that these drugs are direct mitochondrial toxins that inhibit the ETC (Fig. 2A and Additional file 1: Fig. S3C). No change in OCR was observed with didesmethylcariprazine, even at the highest concentration of 10 μM.

Next, we sought to dissociate the toxic off-target effects of the drugs on mitochondria from their on-target effects on the dopamine D2R/D3R. Although these antipsychotics exert functionality at multiple serotonin receptor subtypes, we focused on dopamine receptors since these are the primary therapeutic target linked to the onset of EPS in patients [3, 39]. First, SH-SY5Y cells were treated with an excess concentration of the D2R/D3R agonist dopamine or antagonist haloperidol. Neither of these chemicals induced a decline in basal or maximal OCR (Additional file 1: Fig. S3D). In contrast, a 30 min pre-treatment with haloperidol or dopamine followed by a 30 min treatment with aripiprazole induced a significant decline in basal and maximal OCR. The retention of mitochondrial toxicity under conditions in which

(See figure on next page.)

Fig. 1 Aripiprazole and its primary active metabolite are selectively toxic to galactose-conditioned SH-SY5Y cells. **A** Normalised cellular ATP measurements from glucose- and galactose-conditioned SH-SY5Y cells exposed to the indicated antipsychotic drugs (10 μM), piericidin A, antimycin A (5 μM) or 2-deoxyglucose (2-DG) (50 mM) for 18 h (the data are mean averages ± range from 2 independent experiments with 3 technical repeats; asterisks show the results from one-way ANOVA with Dunnett's multiple comparison test, normalised to control). **B** Normalised cellular ATP measurements from glucose- and galactose-conditioned SH-SY5Y cells treated with the indicated concentrations of aripiprazole or dehydroaripiprazole for 18 h. Data were fitted to the standard dose–effect relationship (activity (%) = = Bottom + (Top − Bottom)/(1 + 10^((LogIC50-X) × HillSlope)) using GraphPad Prism version 8.0 (mean ± SEM from 3 independent experiments, normalised to control). **C** Quantification of cell death in glucose- and galactose-conditioned SH-SY5Y cells treated with increasing concentrations of aripiprazole and dehydroaripiprazole for 18 h (mean ± SEM from 3 independent experiments, asterisks, one-way ANOVA with Dunnett's multiple comparison test, normalised to control) (corresponds to Additional file 1: Fig. S1). **D** Quantification of glucose and galactose-conditioned SH-SY5Y cell proliferative rates following treatment with indicated concentrations of aripiprazole or dehydroaripiprazole over an 86 h period. Proliferation rates were calculated from the linear phase of each growth curve (mean ± SEM from 3 independent experiments, asterisks, one-way ANOVA with Dunnett's multiple comparison test, normalised to control) (corresponds to Additional file 1: Fig. S2)

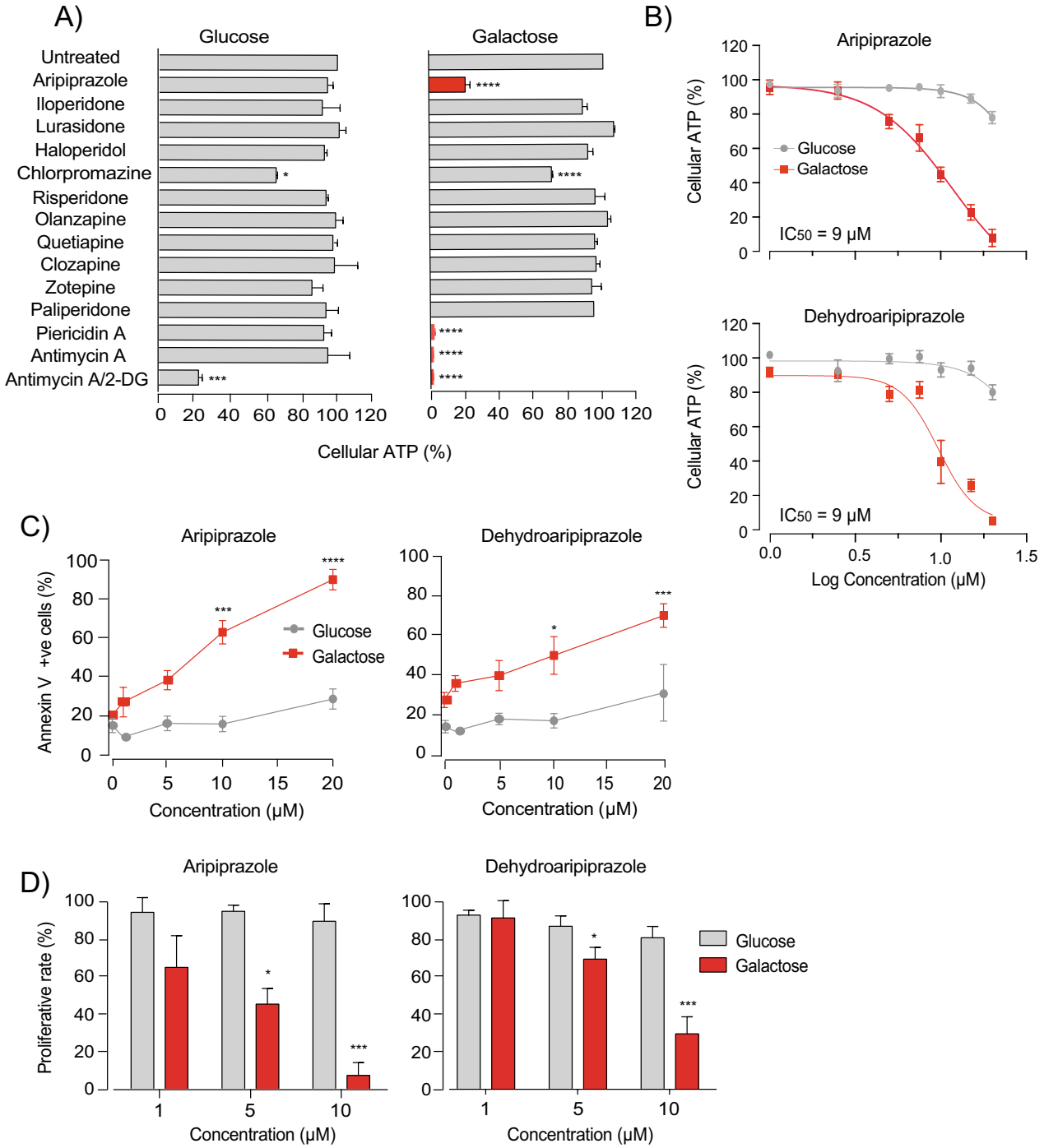

Fig. 1 (See legend on previous page.)

the D2R/D3R are expected to be fully occupied confirms that this is an off-target effect. Furthermore, aripiprazole was also shown to induce significant declines in basal and maximal OCR in human cardiomyocytes (HCMs), despite the fact that these cells express no detectable level of D2R and extremely low levels of D3R (Additional file 1: Fig. S3E, F). We conclude that the drug-induced mitochondrial toxicity observed is independent of D2R/D3R partial agonism.

Next, to determine the molecular mechanism of antipsychotic-induced mitochondrial toxicity, we stimulated plasma-membrane-permeabilised cells with pyruvate and

malate to induce complex I-linked respiration, and with succinate to stimulate complex II-linked respiration (see Additional file 1: Fig. S4A for schematic representation of the ETC). Crucially, we observed a significant decrease in pyruvate/malate-driven respiration following treatment with aripiprazole, dehydroaripiprazole, brexpiprazole and cariprazine (10 μM) (Fig. 2B and Additional file 1: Fig. S4B). Notably, a pre-treatment period of 2 h was required for inhibition by cariprazine to be observed. In contrast, no significant change in succinate-driven respiration was detected with any drug. The same pattern was observed using piericidin A, a specific complex I inhibitor (see Fig. 2C for a schematic of respiratory complex I and the major catalytic sites). To confirm the specificity for complex I, NADH and succinate oxidation rates were measured in bovine mitochondrial membranes. All three antipsychotic drugs, and both primary active metabolites, induced dose-dependent declines in NADH oxidation rate (see Fig. 2D), but did not affect succinate oxidation substantially (Additional file 1: Fig. S4C). Although a significant decrease was observed with cariprazine and dehydroaripiprazole, this was at an excess concentration of 50 μM. Further analyses in bovine sub-mitochondrial particles confirmed that, as expected from its inhibition of the ETC, aripiprazole significantly inhibits ATP synthesis in a dose-dependent manner (Additional file 1: Fig. S4D).

Next, we sought to determine the mechanism of antipsychotic-induced complex I inhibition. Complex I harbours two substrate-binding sites that are both candidate inhibitor binding sites: the NADH-binding site that contains a flavin mononucleotide cofactor (flavin-site) and the ubiquinone-binding site (Q-site) (Fig. 2C). To assess NADH-stimulated flavin-site activity, we measured the reduction rate of the artificial electron acceptors $APAD^+$ and FeCN by the reduced flavin in isolated bovine complex I. We identified no substantial change in the NADH:$APAD^+$/FeCN oxidoreduction rates following exposure to 100 μM aripiprazole, brexpiprazole or cariprazine, clearly demonstrating that the flavin-site is not inhibited (Fig. 2E, F). The artificial ubiquinone analogue decylubiquinone (DQ) was used to assess the Q-site activity in isolated bovine complex I and these data confirmed that each drug induced a substantial decline in NADH:DQ oxidoreduction (Fig. 2G). Therefore, our findings support that dopamine receptor partial agonist antipsychotic drugs are toxic to mitochondria via inhibition of the Q-channel of respiratory complex I.

Third-generation antipsychotics display off-target mitochondrial toxicity in primary mouse neurons

The antipsychotic drugs examined here are designed to modulate dopaminergic neurotransmission in the mesolimbocortical pathways of the human brain. To examine whether the off-target mitochondrial toxicity observed in human neuroblastoma cells is also observed in post-mitotic neurons, primary cultures of forebrain and ventral midbrain neurons were established from wild-type mouse embryos (E13.5). Isolation of these distinctive populations enabled us to compare the propensity for off-target mitochondrial toxicity in dopaminergic versus non-dopaminergic neuronal subtypes.

To confirm the dopaminergic phenotype of ventral midbrain neurons, cells were stained for the specific dopaminergic marker tyrosine hydroxylase (TH). As expected, ventral midbrain neurons stained strongly for TH, whilst forebrain neurons did not express detectable TH (Fig. 3A). Both neuronal subtypes were also stained with β3 tubulin and Hoechst after 7 days in culture, to confirm their viability (Fig. 3B). Cellular ATP levels were then measured in both neuronal subtypes, with and without treatment with each antipsychotic drug for 18 h. A significant decline in cellular ATP (approximately 20%) was observed in ventral midbrain neurons treated with aripiprazole, brexpiprazole and cariprazine (Fig. 3C). In contrast, no change in cellular ATP levels was recorded in forebrain neurons. Treatment with piericidin A significantly reduced ATP production in both midbrain and forebrain neurons (Fig. 3C).

(See figure on next page.)

Fig. 2 Aripiprazole, Brexpiprazole, and Cariprazine directly inhibit respiratory complex I via the Q-channel. **A** Normalised basal and maximal OCR measurements from SH-SY5Y cells treated for 4 h with indicated concentrations of aripiprazole, dehydroaripiprazole, brexpiprazole, cariprazine or didesmethylcariprazine (mean ± SEM from 4 independent experiments, asterisks, one-way ANOVA with Dunnett's multiple comparison test, normalised to control) (corresponds to Additional file 1: Fig. S3C). **B** Normalised OCR measurements driven by complex I substrates (pyruvate/malate) or the complex II substrate (succinate). Permeabilised SH-SY5Y cells were treated with 10 μM aripiprazole, dehydroaripiprazole, brexpiprazole, cariprazine or 5 μM piericidin A, antimycin A (mean ± SEM from 4 independent experiments, asterisks, one-way ANOVA with Dunnett's multiple comparison test, normalised to control) (corresponds to Additional file 1: Fig. S4B). **C** A cartoon depiction of mammalian complex I structure with the two substrate-binding sites indicated. **D** Normalised NADH:O_2 oxidoreduction rates of bovine mitochondrial membranes exposed to varying concentrations of aripiprazole, brexpiprazole, cariprazine, dehydroaripiprazole and didesmethylcariprazine. Respective IC_{50} values from the standard dose–effect relationship (see "Methods" Section) are indicated in brackets. **E** Normalised NADH:$APAD^+$, **F** NADH:FeCN, and **G** NADH:DQ oxidoreduction rates of isolated bovine complex I exposed to 100 μM aripiprazole, brexpiprazole, cariprazine or 1 μM piericidin A (mean ± SEM from 3 independent wells per treatment, asterisks, one-way ANOVA with Dunnett's multiple comparison test, normalised to control)

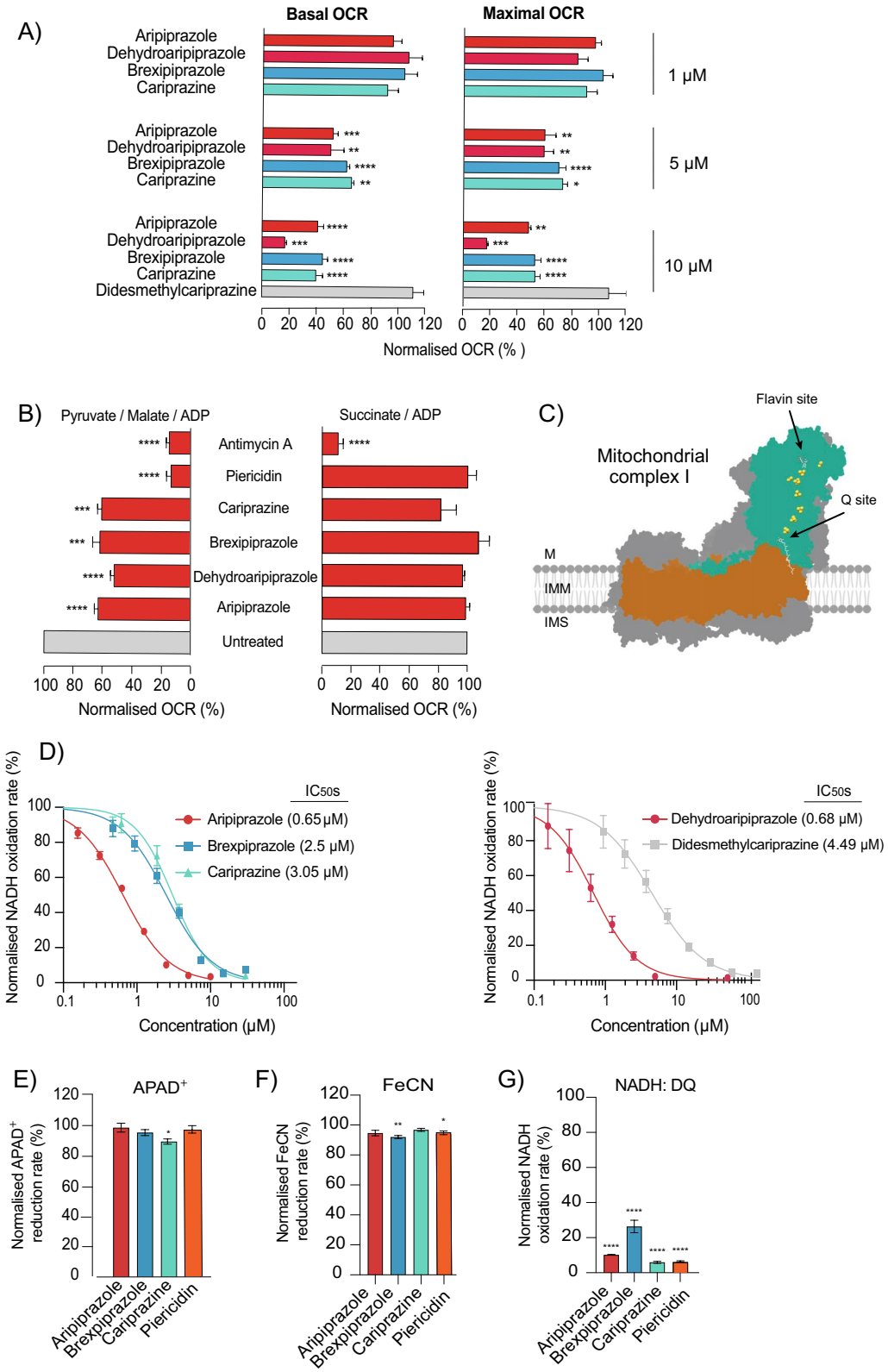

Fig. 2 (See legend on previous page.)

Importantly, analyses of NADH oxidation rate in mouse mitochondrial membranes demonstrated that all drugs of interest retained their inhibitory effects on complex I-linked respiration (Additional file 1: Fig. S5A), confirming that mitochondrial toxicity is conserved across species. Next, we measured the direct effects of each antipsychotic drug on mitochondrial respiratory function. Crucially, each compound induced a significant decline in basal and maximal OCR in midbrain neurons (Fig. 3D and Additional file 1: Fig. S5B). In contrast, while no statistically significant change in basal OCR was detected with either antipsychotic drug in forebrain neurons, a substantial and significant decline in maximal OCR was still recorded (~28% aripiprazole, ~42% brexpiprazole, ~26% cariprazine). The fact that aripiprazole, brexpiprazole and cariprazine had different effects on the two cell types indicates differential rates of uptake and accumulation—perhaps increased in the ventral midbrain neurons resulting from their unmyelinated nature [40].

Aripiprazole induces mitochondrial toxicity in *Drosophila melanogaster*

To explore the mitochondrial liabilities of third-generation antipsychotics in a living organism, we employed *Drosophila melanogaster* as an in vivo model. *Drosophila* also have the advantage that, effects on dopamine signalling can be distinguished from effects on mitochondrial function. To confirm that mitochondrial toxicity was conserved in flies, *Drosophila* S2 cells and mitochondria isolated from *Drosophila* were treated with aripiprazole, brexpiprazole and cariprazine for 4 h and 15 min, respectively. All drugs induced a significant decline in basal OCR (20–34%) and maximal OCR (27%-74%) in S2 cells (Additional file 1: Fig. S6A, B). Acute drug treatment also decreased basal OCR (and in the case of aripiprazole and brexipiprazole maximal OCR) of isolated mitochondria from *Drosophila*, while the canonical complex I inhibitor piericidin A completely abolished mitochondrial respiration (Additional file 1: Fig. S6C, D). Taken together, these data demonstrate that third-generation antipsychotic drugs induce mitochondrial toxicity in *Drosophila melanogaster*, demonstrating the utility of this model for our study.

Due to limitations in compound availability, aripiprazole was the only drug investigated in behavioural analyses. First, it was important to distinguish the on-target versus off-target effects of aripiprazole in *Drosophila.* That is, behavioural/functional effects caused by the partial agonist interaction of aripiprazole with its primary therapeutic target (D2R/D3R) versus interaction with an unintended molecular target (e.g. mitochondrial complex I). In *Drosophila,* dopamine acts as an arousal signal by downregulating the activity of the dorsal layer of fan-shaped body (dFB) neurons, an effector component of the sleep homeostat [41]. Sleep fragmentation correlates with increased dopamine signalling in flies and can be measured by monitoring the activity of individual flies [42]. Therefore, we used sleep fragmentation as a way to measure the on-target effect of the drug. Accordingly, significant increases in the number of inactivity episodes were detected in aripiprazole-fed flies after 14 and 21 days of exposure (Fig. 4A).

Mitochondrial dysfunction in the skeletal muscle has been shown to impair motor performance in *Drosophila* [43]. To assess the effect of mitochondrial complex I inhibition on this phenotype, we measured the climbing ability of adult flies fed with aripiprazole or the canonical complex I inhibitor rotenone for varying amounts of time: with climbing latency defined as the amount of time taken for 5 flies (out of 20) to reach a 15 cm height marker within a vertical chamber. Therefore, an increase in climbing latency reflects impaired locomotion. Although no climbing impairment was noted in aripiprazole-fed flies after 5 or 14 days feeding, a significant increase in climbing latency was detected after 21 and 28 days (Fig. 4B). A robust and significant increase in climbing latency was also detected in flies exposed to rotenone for 5 days (later time-points are not shown, as flies did not survive the treatment). Finally, we investigated the effect of aripiprazole treatment on the ultrastructure of mitochondria in the brain and thoracic muscle of adult flies. Various studies have shown DMSO to be toxic to flies, with 0.5% DMSO only appearing to induce damage in our study following chronic feeding [44]. Although

(See figure on next page.)

Fig. 3 Aripiprazole, brexpiprazole and cariprazine are toxic to primary neonatal mouse neurons. **A** Representative image of a sagittal section from an embryonic mouse brain (e13.5) stained with an anti-tyrosine hydroxylase (TH) antibody to highlight dopaminergic neurons (white arrow). Dashed yellow boxes represent the ventral midbrain and forebrain areas used to prepare neurons. **B** Representative confocal images of ventral midbrain and forebrain neurons (e13.5) maintained for 7 days and stained with Hoechst (blue) and an antibody to β3 tubulin (green). **C** Normalised cellular ATP measurements from mouse embryonic (e13.5) ventral midbrain and forebrain neurons. Neurons cultured for 7 days were exposed to aripiprazole, brexpiprazole, cariprazine or piericidin A (5 μM for 18 h) (mean ± SEM from 5 independent experiments, asterisks, one-way ANOVA with Dunnett's multiple comparison test, normalised to control). **D** Normalised basal and maximal OCR measurements from mouse ventral midbrain and forebrain neurons (e13.5) grown for 7 days and treated with aripiprazole, brexpiprazole, cariprazine or piericidin A (5 μM for 4 h) (corresponds to Additional file 1: Fig. S5B) (mean ± SEM from 5 independent experiments, asterisks, one-way ANOVA with Dunnett's multiple comparison test, normalised to control)

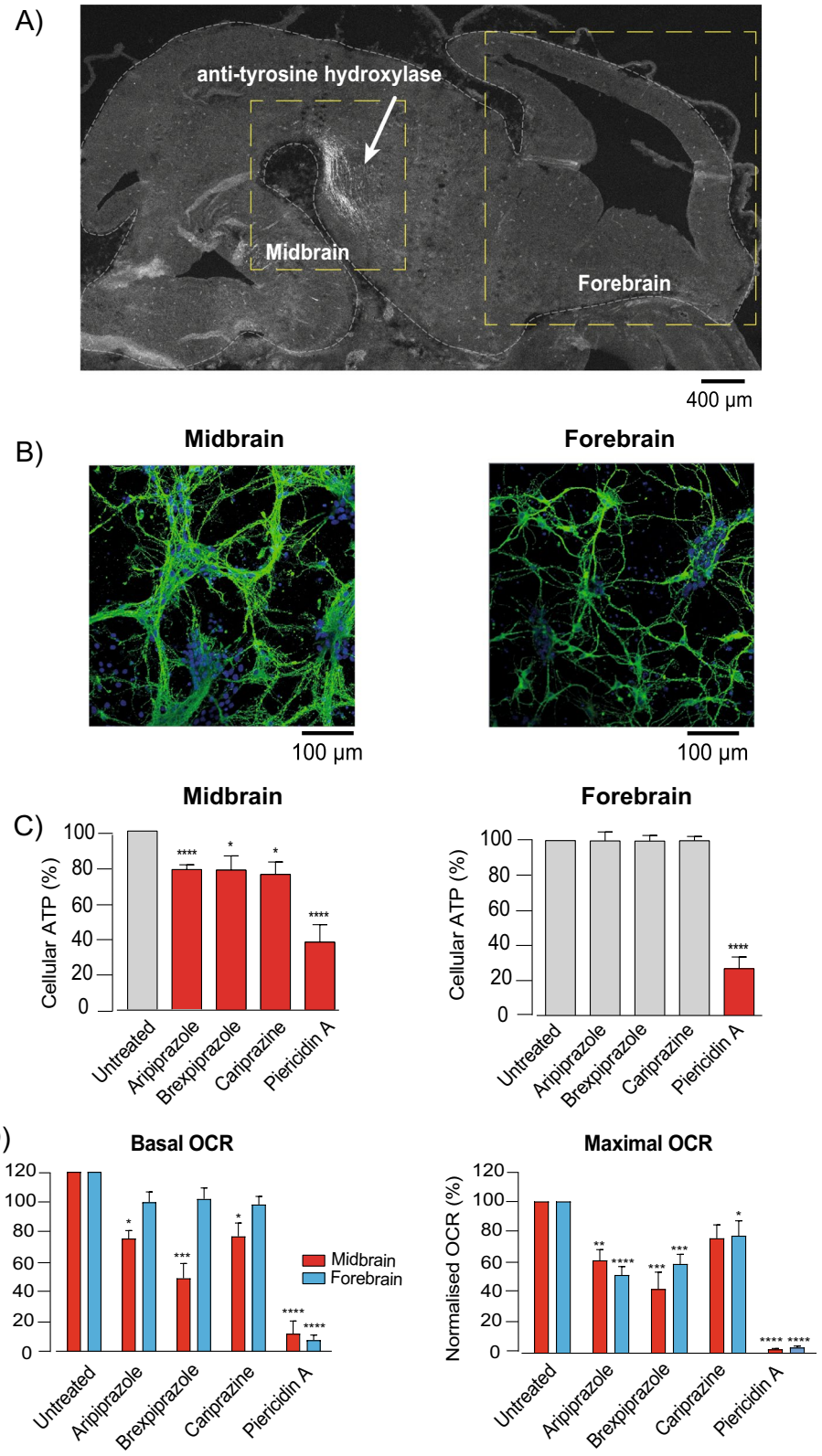

Fig. 3 (See legend on previous page.)

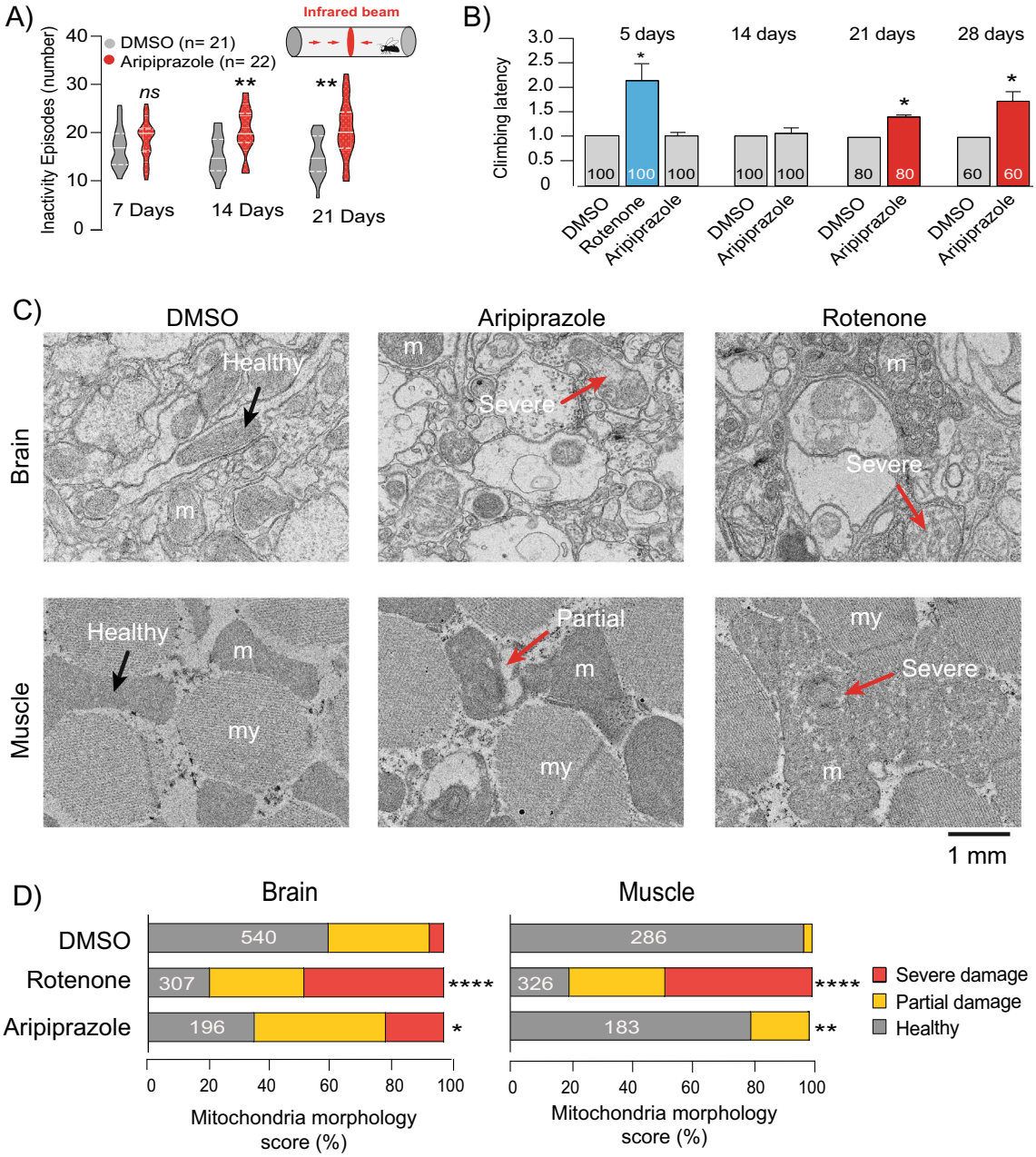

Fig. 4 Aripiprazole causes motor dysfunction and mitochondrial defects in adult flies. **A** Total activity of adult flies treated with DMSO (0.5% v/v) or aripiprazole (1 mM), measured for indicated periods using a Trikinetics system (*n* = number of flies per test group, asterisks, two-way ANOVA with the Tukey multiple comparison test). **B** Climbing performance of adult flies fed with DMSO (0.5% v/v) rotenone or aripiprazole (1 mM) for indicated periods. Total number of flies tested per group are indicated on the graph (mean ± SEM from 3 independent experiments, asterisks, two-tailed unpaired *t*-test). **C** Representative TEM images of brain and thoracic muscle from adult flies treated with DMSO (0.5%) or aripiprazole (1 mM) for 28 days or rotenone (1 mM) for 5 days (arrows, examples of the scoring criteria for the morphological assessment, m = mitochondria, my = myofibrils). **D** Quantification of mitochondrial damage. The total number of mitochondria scored in each sample group is indicated (samples pooled from 2 flies per treatment, chi-squared analysis with Bonferroni correction)

rotenone induced clear perturbations in mitochondrial ultrastructure, with abundant cristae fragmentation present in both brain and thoracic muscle after 5 days feeding, no significant damage was detected with aripiprazole (Additional file 1: Fig. S6E). In comparison, clear abnormalities in mitochondrial ultrastructure were evident in the brain and thoracic muscle of aripiprazole-fed flies after 28 days (Fig. 4C, D). Clear areas of vacuolisation

were detected in ~ 20% of densely packed mitochondria in thoracic muscle, with no concurrent damage to myofibrils being noted. Similarly, a significant number of brain mitochondria (~ 20%) presented with fragmented cristae following 28 days aripiprazole feeding, with a mixture of partial and severe damage being observed (Fig. 4C, D). It should be noted that ~ 40% of mitochondria appeared damaged in the brains of flies fed DMSO for 28 d, and the amount of damage induced by aripiprazole was calculated relative to this value. Taken together, our data show that in vivo exposure to aripiprazole results in mitochondrial ultrastructural damage in both the brain and thoracic muscle of adult flies, which is linked with impaired motor performance.

Discussion

First-generation antipsychotic drugs are potent D2R antagonists inducing severe and high-frequency EPS (~ 30 to 70% of all patients) [10, 11, 45]. To improve tolerability and lessen patient suffering, the D2R/D3R partial agonists aripiprazole, brexpiprazole and cariprazine were developed, with this novel MoA promoting favourable drug side-effect profiles. However, adults taking these drugs still exhibit a high incidence (~ 5 to 15%) of EPS in both clinical trials and real-world analyses [16, 21, 46–48]. EPS were similarly high (~ 15 to 25%) in the clinical trials of paediatric patients (10–17 years) treated with oral aripiprazole for bipolar mania, demonstrating that neurological toxicity is conserved from children to adults [21]. Moreover, EPS are irreversible in some adults and children after discontinuation of third-generation antipsychotic drugs, suggesting these medications comprise toxic properties that can inflict permanent neuronal damage [23, 24]. Given that dopamine receptor partial agonists are prescribed to millions of patients globally each year, it is crucial to better understand why EPS remain a considerable liability for these medications and to delineate if they are driven by on- or off-target pharmacology. Here, we investigated if aripiprazole, brexpiprazole and cariprazine affect mitochondrial function (respiration), and explored the possible contribution of this effect to human EPS.

Our data show that aripiprazole, brexpiprazole and cariprazine are direct inhibitors of the ETC in cells (SH-SY5Y cells and primary mouse neurons) and mitochondrial membranes (bovine and mouse). In a cellular context, none of the other antipsychotic medications screened here induced mitochondrial toxicity. Whilst our findings are contrary to previous reports that detected inhibition of the ETC by a wider range of antipsychotic compounds, the earlier studies were limited to cell-free purified mitochondrial systems [49, 50]. We propose that first and second-generation antipsychotic compounds cannot gain access to their molecular target(s) in mitochondria in intact cellular systems, as tested here. This underlines the importance of combining mitochondrial toxicity data in cell-free and intact cellular assays [49–53]. Using functional assays on respiratory complexes, we show the three partial agonists specifically inhibit the site of ubiquinone reduction (Q-site) in mitochondrial complex I. We present strong evidence to show that this mitochondrial inhibition is off-target and disconnected from the on-target pharmacology of third-generation antipsychotic drugs. All three compounds inhibit complex I activity in isolated complex I, cell-free purified mitochondrial membranes and intact cellular systems. In contrast, respiration in cells is not inhibited following treatment with dopamine (full agonist of D2R and D3R) or haloperidol (D2R and D3R antagonist). Importantly, aripiprazole, brexpiprazole and cariprazine inhibit mitochondrial respiration in both primary neurons and non-neuronal cells (human cardiomyocytes) that lack D2R expression.

In vivo studies using *Drosophila melanogaster* showed that chronic feeding with aripiprazole resulted in significant climbing defects after 21 d, which closely paralleled the emergence of severely damaged mitochondria in the thoracic muscle and brain. These defects further deteriorated during 21–28 days treatment, suggesting that aripiprazole elicits degenerative toxicity. Importantly, the delayed onset of locomotor dysfunction in flies mirrors aripiprazole clinical data, with EPS typically presenting weeks-to-months after initiating aripiprazole treatment. The canonical complex I inhibitor rotenone also induced mitochondrial cristae fragmentation and locomotor dysfunction, albeit with significantly faster onset. These differential rates of toxicity between rotenone and aripiprazole are expected, because rotenone more potently inhibits complex I compared to aripiprazole (IC50 value of 6.9 nM using bovine mitochondrial membranes, more than 100× lower than aripiprazole [54]). Crucially, we detected our on-target D2R-dependent marker (i.e. increased inactivity episodes) at an earlier time-point (14 days) compared to the climbing defects (21 days), confirming that mitochondrial toxicity is disconnected from D2R/D23R partial agonism in a living organism.

Although further studies are required to unequivocally show that motor side-effects are a direct consequence of mitochondrial inhibition, further evidence exists to support this proposal. Aripiprazole occupies approximately 95% of D2Rs/D3Rs in the human striatum (≥ 14 days treatment), with extremely strong binding affinities (K_i = 0.34 nM for D2R and 0.8 nM for D3R, among the highest recorded for any antipsychotic drug [55, 56]). A lower dopamine receptor occupancy (75–80%) by first-generation antipsychotics (i.e. D2R/D3R antagonists)

promotes serious EPS [57–59]. Therefore, if aripiprazole does induce motor disorders by D2R/D3R partial agonism, it is surprising that the prevalence is relatively low. This alone suggests that an alternative off-target mechanism is responsible for driving aripiprazole-induced neurotoxicity and associated EPS.

We next considered if the mitochondrial inhibition reported here could contribute to clinical EPS. In SH-SY5Y cells and mouse neurons, respiration was significantly inhibited at concentrations of 5 μM and above. Although levels in patient serum are reported to be in the range of 0.1–1.3 μM (aripiprazole), 0.2–0.5 μM (brexpiprazole), and 0.09–0.4 μM (cariprazine) [37, 60–62], a pharmacokinetic study in mice showed that aripiprazole accumulated by approximately ninefold greater levels in the brain (relative to serum levels) [63]. Brain accumulation has also been reported for other antipsychotics, such as haloperidol [64]. If this drug distribution behaviour translates into humans, partial agonists may concentrate at mitochondrial toxic levels and drive EPS. In mouse studies, the P-glycoprotein has been shown to regulate aripiprazole brain levels as it controls drug efflux; polymorphisms in this transporter may further sensitize particular patient groups to higher drug accumulation and toxicity [63, 65]. Similarly, patients with pre-existing mitochondrial impairment (e.g. those with mitochondrial disease) are likely to be particularly susceptible to aripiprazole-induced mitochondrial toxicity [66]. It would also be interesting to investigate whether specific mitochondrial DNA (mtDNA) haplotypes are correlated with an increased incidence of EPS following aripiprazole treatment: for example haplotypes conferring a predisposition to PD or reduced mitochondrial bioenergetic function [67–70].

We next considered how aripiprazole, brexipiprazole and cariprazine inhibit complex I. Recently IACS-2858, a structural analogue of the anti-cancer agent IACS-010759 currently in phase 1 clinical trials for acute myeloid leukaemia and solid tumours, was shown to inhibit complex I by binding tightly to a new inhibitory site near the entrance of the Q-site; thereby it inhibits ubiquinone reduction by a 'cork in bottle' mechanism [71]. Binding is mediated by a skeleton of aromatic/nonaromatic rings, with a similar architecture to the complex I inhibitors mubritinib and carboxyamidotriazole [72]. Third-generation antipsychotic drugs also contain chains of aromatic and nonaromatic rings within their chemical backbone and therefore may also bind to the IACS-2858-site. Accordingly, we performed molecular docking analysis (Additional file 1: Fig. S7). Interestingly, when aripiprazole, brexipiprazole and cariprazine were flexibly aligned to the fixed conformation observed in the IACS-bound mouse complex I cryo-EM structure (PDB: 7B93), they could be accommodated in the site, with protein–ligand interaction energies in line with equivalent values calculated here for IACS-2858 as well as mubritinib and carboxyamidotriazole (Additional file 1: Fig. S7I). The same region of the site has also been observed, in different cryo-EM structures, to contain an adventitiously-bound detergent [73], a rotenone molecule and short-chain ubiquinone species [74], suggesting it is a good candidate for off-target drug binding. However, future structural studies are vital to unequivocally delineate how aripiprazole, brexipiprazole and cariprazine inhibit complex I. It will also be important to test substructures and closely related structural analogues to identify the chemistry conferring complex I binding; if such changes in chemistry are not essential for D2R-D3R binding, chemical modification may represent a possible means to dial-out off-target mitochondrial toxicity from these third-generation antipsychotics.

In conclusion, our results show that the third-generation antipsychotics aripiprazole, brexpiprazole and cariprazine induce off-target mitochondrial toxicity via selective inhibition of the Q-site of mitochondrial complex I. Whilst these drugs exhibit a more favourable side-effect profile relative to other antipsychotics, they still carry an unexpectedly high risk of EPS in adults and adolescents [75]. We present novel and robust mechanistic toxicology data that may reconcile these clinical observations, given that complex I inhibition and mitochondrial dysfunction are strongly connected to motor dysfunction in neurodegenerative disease. To strengthen our understanding of the in vitro-to-clinic translation, further studies are essential that measure aripiprazole concentrations in the human brain (particularly in those patients experiencing debilitating EPS) and it will be of great interest to monitor the incidence of EPS if novel partial agonists are developed that lack complex I inhibition. These data will be critical to resolving the contribution of mitochondrial toxicity to clinical EPS and decreasing the incidence of sideeffects from antipsychotic medications.

Materials and methods

Materials

Aripiprazole, Clozapine, Quetiapine, Olanzapine, Paliperidone, Risperidone and Rotenone (Abcam), Dehydroaripiprazole (Santa Cruz Biotechnology), Didesmethylcariprazine (Clearsynth), Haloperidol, Iloperidone, Lurasidone, Zotepine (Sigma), Brexpiprazole and Cariprazine (Cayman Chemicals) were dissolved to desired stock concentrations in DMSO. Chlorpromazine (Sigma) was dissolved in distilled water, while Antimycin A, FCCP, Oligomycin A (Sigma) and Piericidin A (Cayman Chemicals) were dissolved in ethanol. All drug stock

solutions were diluted into appropriate cell culture media to desired concentrations.

Cell culture

The human neuroblastoma cell line SH-SY5Y (ATCC #CRL-2266) was maintained in Dulbecco's Modified Eagle Medium/Ham's Nutrient Mixture F12 (DMEM) (#31331028, Gibco), supplemented with 10% heat-inactivated Fetal Bovine Serum (FBS) and 1 mM sodium pyruvate (Gibco) at 37 °C, 5% CO_2 in a humidified incubator. Cells were routinely passaged twice weekly. Primary Human Cardiomyocytes (HCMs; PromoCell) were maintained in myocyte growth medium (PromoCell), supplemented with 11 mM glucose and supplement mix (5% FCS, 0.5 ng mL^{-1} epidermal growth factor, 2 ng mL^{-1} basic fibroblast growth factor and 5 µg mL^{-1} insulin). Cells were maintained at 37 °C, 5% CO_2 in a humidified incubator and passaged once per week. *Drosophila* Schneider 2 (S2) cells (Thermofisher) were maintained in Schneider's *Drosophila* Medium (Gibco) supplemented with 10% FCS, at 26 °C in a non-CO_2 incubator. Semi-adherent cells were passaged twice weekly when approximately 85–90% confluence was reached.

Glucose to galactose metabolic switching

SH-SY5Y cells were switched from standard growth medium to glucose-free DMEM (#11966025, Gibco) supplemented with 11 mM glucose or galactose, 10% FBS and 1 mM sodium pyruvate. Cells were grown in glucose or galactose-supplemented media for a period of 72 h prior to drug treatment.

Isolation and culture of primary mouse neurons

Ventral midbrain and forebrain [76, 77] neurons were dissected from the brains of wild type (C57BL/6) day E13.5 mouse embryos, as previously described [76]. Neurons were dissected in ice-cold DMEM + GlutaMAX (#10566016, Gibco) medium supplemented with 5% FBS. Following dissection, neurons were mechanically dissociated and then enzymatically digested using 1 × TrypleExpress for 2 min at 37 °C. Dissociated midbrain and forebrain neurons were resuspended in neurobasal medium, prepared as previously described [78] and centrifuged at 200×*g* for 5 min. Neurons were then seeded at the indicated densities into opaque 96-well tissue culture microplates (Corning™), Seahorse XF96 microplates (Agilent) or glass coverslips coated with Poly-D-lysine (50 µg ml^{-1}, Sigma) in 24-well plates (Corning™). Neurons were maintained at 37 °C in a humidified 5% CO_2 incubator for 7 days, with medium supplemented every 2–3 days.

ATP assays

SH-SY5Y cells cultured in glucose or galactose-containing DMEM medium were seeded into opaque 96-well tissue culture microplates (Corning™) at a density of 2×10^4 per well and incubated at 37 °C, 5% CO_2 for 24 h. For experiments using primary neurons, mouse embryonic forebrain and ventral midbrain neurons were seeded at densities of 7.5×10^4 and 1×10^5 per well, respectively, and allowed to grow for 7 days at 37 °C, 5% CO_2. On the day of the assay, media was aspirated from cells, and drugs added directly for a period of 18 h. Total cellular ATP was then measured using the Promega CellTiter-Glo® luminescent cell viability assay (#G7571), according to the manufacturer's protocol. The average concentration of ATP (calculated from triplicates for each condition) was normalised to the average amount of ATP produced by DMSO-treated cells for each biological replicate. Data were fit to the standard dose–effect relationship (activity (%) = Bottom + (Top–Bottom)/(1 + 10^((LogIC50-X)*HillSlope)) using GraphPad Prism version 8.0.

Cell proliferation assays

Cell proliferative capacity was measured in real-time using the xCELLigence® system (RTCA DP instrument; ACEA Biosciences), according to manufacturer's instructions. SH-SY5Y cells were seeded into xCELLigence E-plates (ACEA Biosciences) at a density of 2.0×10^4 cells/well (glucose-cultured cells) and 5.0×10^4 cells/well (galactose-cultured cells) and incubated at 37 °C, 5% CO_2, while impedance values (expressed as total cell index) were automatically monitored by the xCELLigence system. After an initial growth period of 24 h, impedance readings were paused to allow for addition of drugs to cells, and then resumed for a further 86 h. Average proliferative rates were calculated from the linear region of each growth curve, from triplicates per condition per biological replicate. These, along with final cell index values after the 110 h total growth period were normalised against those of DMSO-treated cells.

Extracellular flux analyses

Measurements of real-time of oxygen consumption rates (OCR) were determined in whole cells using a Seahorse XF96 extracellular flux analyser (Agilent) as described previously [79], with the following modifications. SH-SY5Y cells were seeded into Seahorse XF96 microplates (Agilent) pre-coated with rat-tail collagen (30 µg ml^{-1}, Sigma) at a density of 3.0×10^4 cells/well in glucose-supplemented DMEM medium (containing 10% FBS, 1 mM sodium pyruvate). HCMs were seeded into uncoated XF96 microplates in glucose-supplemented myocyte

growth medium at a density of 1.5×10^4 per well. Mouse embryonic ventral midbrain and forebrain neurons were seeded into XF96 microplates pre-coated with Poly-D lysine, in neurobasal medium, at densities of 1.5×10^5 cells/well and 1×10^5 cells/well, respectively, and allowed to grow for 7 d. All cell types were incubated at 37 °C, 5% CO_2 for 16 h after seeding. *Drosophila* S2 cells were seeded into uncoated XF96 microplates in Schneider's medium at a density of 3.0×10^4 per well, and incubated at 28 °C for 16 h without CO_2.

On the day of the assay, growth medium was removed, and cells washed 3X in unbuffered serum-free DMEM Seahorse Assay Medium (32 mM NaCl, 2 mM GlutaMAX, 1 mM sodium pyruvate, 11 mM glucose). Cells were placed into a 37 °C non-CO_2 incubator for 1 h (apart from *Drosophila* S2 cells which were kept in a 28 °C non-CO_2 incubator). Antipsychotic drugs, diluted in Seahorse Assay medium to desired concentrations, were added directly, with cells then being incubated at 37 °C in a non-CO_2 incubator for 4 h. Following incubation, cells were placed into the Seahorse XF96 Analyser and OCR recorded, with canonical mitochondrial toxins injected sequentially at the indicated time-points. The canonical mitochondrial toxins oligomycin A (ATP synthase inhibitor), FCCP (mitochondrial uncoupler) and antimycin A with rotenone (complex III and I inhibitors, respectively) were loaded into sensor cartridge injection ports (Agilent) to yield final concentrations of 2 µM oligomycin A, rotenone, antimycin A and 500 nM FCCP for SH-SY5Y cells and 5 µM oligomycin A, 2 µM rotenone, antimycin A for mouse embryonic ventral midbrain and forebrain neurons. FCCP was added at 1 µM to forebrain neurons and 2 µM to ventral midbrain neurons. For HCMs, 2 µM oligomycin A, rotenone, antimycin A and 4 µM FCCP were used. Basal OCR was calculated by subtraction of antimycin A-independent OCR from the baseline OCR, prior to oligomycin A addition. Maximal OCR was calculated following by subtracting antimycin A-independent OCR from FCCP-stimulated OCR. Values were averaged from independent experiments (six technical replicates of each condition per experiment) and expressed as a percentage of those calculated for DMSO-treated cells. OCR measurements were made at 28 °C for *Drosophila* S2 cells, and 37 °C for all other cell types.

Measurement of electron transport chain complex activity in permeabilised cells

To assess the activity of individual respiratory complexes in SH-SY5Y cells, cholesterol-dependent Permeabiliser XF Plasma Membrane Permeabiliser (PMP; Agilent) was used, essentially as described previously [80]. To assess complex I activity, 10 mM pyruvate, 2.5 mM malate and 1 mM ADP were injected into sensor cartridge ports, to stimulate complex I-linked respiration. This was followed by the injection of 2 µM piericidin A (to abolish complex I activity), followed by injection of 10 mM succinate and 1 mM ADP to stimulate complex II-linked respiration. All substrates were diluted in 1×Mitochondrial Assay Solution (MAS) buffer consisting of 70 mM sucrose, 220 mM mannitol, 10 mM KH_2PO4, 5 mM $MgCl_2$, 2 mM HEPES, 1 mM EGTA, at pH 7.4. Prior to assay, cells were washed twice in MAS buffer and drugs, diluted to desired concentrations in MAS buffer, immediately added to cells. PMP was then added directly at a final concentration of 1 nM in order to permeabilize the plasma membrane, whilst leaving mitochondrial membranes intact. OCR measurements were made using a Seahorse XF96 Analyser, with antimycin A-insensitive OCR subtracted from pyruvate/malate/ADP-stimulated OCR and succinate/ADP-stimulated OCR to give final OCR measurements for complex I and II-linked respiration. These values were then normalised to those obtained from DMSO-treated cells.

Biochemical enzyme activity assays

All catalytic activity assays were conducted at 32 °C in 96-well plates using a Molecular Devices Spectramax 384 plus plate reader unless otherwise stated. Linear rates were measured for all assays, inhibitors added from DMSO stock solutions as required, and relevant inhibitor-insensitive rates measured using 1 µM piericidin A. Bovine and mouse membranes were prepared as described previously [81, 82], diluted to 20 µg mL^{-1} in 10 mM Tris-SO_4 (pH 7.5) and 250 mM sucrose and supplemented with 3 µM horse heart cytochrome *c* (Sigma Aldrich). For measurement of NADH:O_2 oxidoreduction, catalysis was initiated by addition of 200 µM NADH and monitored at 340 and 380 nm ($\varepsilon_{340-380}=4.81$ mM^{-1} cm^{-1}). Succinate oxidation was determined using a coupled enzyme assay [83] in the presence of 5 mM succinate, 60 µg mL^{-1} FumC, 300 µg mL^{-1} MaeB, 2 mM $MgSO_4$, 1 mM K_2SO_4 and 2 mM $NADP^+$. Bovine complex I was purified as described previously [84], and diluted to 0.5 µg mL^{-1} in 20 mM Tris–HCl (pH 7.5), 0.15% soybean asolectin (Avanti Polar Lipids) and 0.15% 3-[(3-Cholamidopropyl)dimethylammonio]-1-propanesulfonate (CHAPS, Merck Chemicals Ltd.). NADH:decylubiquinone (DQ), NADH:3-acetylpyridine adenine dinucleotide ($APAD^+$), and NADH:ferricyanide (FeCN) oxidoreduction by complex I were measured using 200 µM NADH and 200 µM DQ, 100 µM NADH and 500 µM $APAD^+$, or 100 µM NADH and 1 mM FeCN, respectively. Kinetic data were fit to the standard dose–effect relationship (activity (%) $=100/(1+(IC_{50})/([\text{inhibitor}])^{\text{Hill slope}})$ using GraphPad Prism version 8.0, and IC_{50} values are reported with their standard errors.

Sub-mitochondrial particles (SMPs) were prepared as described previously [82], and diluted to 10 μg mL^{-1} in 10 mM Tris-PO_4 (pH 7.5), 250 mM sucrose and 2 mM $MgCl_2$. ATP synthesis quantification was adapted from a previously described protocol [85]. Briefly, the assay was performed at 20 °C using a Glomax 20/20 luminometer (Promega) by the luciferin/luciferase system supplemented with 25 μM P1,P5-di(adenosine-5′) pentaphosphate (AP5A; Sigma Aldrich), 3 μM IF1 (prepared as described previously [86], 100 μM ADP, and 20 μg mL^{-1} luciferase reagent (ATP Bioluminescence Assay Kit CLS-II, Roche). The reaction was initiated with 200 μM NADH, luminescence measured for 10 min, and the first derivatives calculated for the ATP synthesis rate.

Cell death analyses

Cell death was assessed as described previously [87], with the following modifications. Glucose and galactose-cultured SH-SY5Y cells were seeded into 6-well plates (Corning™) at a density 7.0×10^5 cells/well, incubated for 24 h at 37 °C, 5% CO_2 and drugs then added at desired final concentrations, in glucose or galactose-medium. After 18 h treatment, cells were collected by trypsinisation and resuspended in glucose or galactose-medium, to allow recovery for 20 min at 37 °C, 5% CO_2. Cells were then diluted 1:5 in annexin binding buffer (1.8 mM $CaCl_2.2H_2O$, 1 mM $MgCl_2$ $0.6H_2O$, 5 mM KCl, 150 mM NaCl, 10 mM HEPES/NaOH, pH 7.4), followed by the addition of diluted Annexin V-FITC (synthesised in-house [88]) and incubated for 30 min in the dark at room temperature. Samples were then placed on ice and 1 μl of the membrane impermeable, far-red fluorescent dye DRAQ7 (BioStatus) added to detect late-stage apoptotic or necrotic cells. Samples were analysed immediately using a BD FACSCanto™II (BD FACSDiva software) to quantify cell death.

Western blotting

SH-SY5Y cells cultured in glucose-supplemented DMEM were seeded into 6-well tissue culture plates at a density of 7.5×10^5 cells/well, while HCMs were seeded at a density of 1.3×10^5 cells/well. Cell lysates were prepared in ice-cold RIPA buffer (Thermo Scientific™. #89901) supplemented with 100X Halt Protease and Phosphatase inhibitor cocktail for 15 min (Thermo Scientific™.#78440), and then centrifuged for 10 min at 13,000×*g*, 4 °C. Supernatant protein concentrations were normalised using a BCA protein assay (Pierce), according to the manufacturer's protocol. Samples were prepared by diluting lysates in loading buffer containing 1% sodium dodecyl sulphate with β-mercaptoethanol, and heated for 5 min at 70 °C. These were run on 4–12% Criterion protein gels (Bio-Rad) at 100 V for 1 h. Proteins were blotted onto nitrocellulose membranes using Trans-Blot® Turbo™ Transfer System (Bio-Rad. #1704150). Membranes were blocked for 1 h at room temperature in buffer consisting of TBST (0.1% Tween-20, 10 mM Tris–HCl, 150 mM NaCl) and 5% dried skimmed milk powder (Marvel). Membranes were probed with primary antibodies against dopamine D2 receptor (Abcam, ab85367), dopamine D3 receptor (Abcam, ab155098), and vinculin (Abcam, ab130007), for 16 h at 4 °C. This was followed by a 1 h incubation at room temperature with anti-mouse or anti-rabbit secondary antibodies conjugated with horseradish peroxidase (HRP; Sigma, A8924). Blots were developed using a Konica SRX101A X-ray Film Processor.

Immunofluorescence

For analysis of TH expression in the mouse ventral midbrain and forebrain, whole brains from E13.5 embryos were cryosectioned on sagittal planes, fixed with 2% PFA for 30 min at room temperature, and then simultaneously permeabilised and blocked for 30 min at room temperature with a buffer containing 10% donkey serum (Jackson ImmunoResearch, UK) and 0.1% Triton X-100 (Sigma). Rabbit anti-tyrosine hydroxylase (TH) was added overnight in blocking solution at 4 °C to whole brain cryosections. The next day, neurons were washed in PBS and incubated in the dark for 1 h with donkey anti-rabbit Alexa Fluor 555 (1:500). Neurons were washed 3 times in PBS then stained with Hoechst to identify nuclei. Stained cells were imaged using a confocal microscope (LSM 880, Zeiss).

Drosophila strains

Fly stocks were maintained on standard cornmeal agar media at 25 °C. The strain used was w^{1118}. All behavioural experiments on adult flies were performed using males.

Isolation of fly mitochondria

Mitochondria were isolated from freshly eclosed adult *Drosophila,* according to the manufacturer's protocol (Sigma). Briefly, 50 flies (male and female) were placed onto ice and gently homogenized using a Dounce homogenizer, with 10 strokes per extraction. This was followed by a 5 min centrifugation of supernatants at 600×*g* and 10 min centrifugation at 11,000×*g*, 4 °C. Pellets were resuspended in complex I assay solution (1X MAS buffer supplemented with 10 mM pyruvate and 5 mM malate) at 4 °C, and total protein content normalized using a Bradford assay.

Behavioural analyses in *Drosophila*

Freshly eclosed male flies were maintained on standard cornmeal agar media supplemented with 1 mM aripiprazole, 1 mM rotenone or 0.5% (v/v) DMSO for 5, 14, 21 or

28 days. For the climbing assay, 20 male flies were placed into glass columns (23 cm long, 2.5 cm in diameter) that were lined with nylon mesh (250 µm, Dutscher Scientific) and marked with a line at 15 cm. After a 30–60 min recovery from CO_2 anaesthesia, flies were gently tapped to the bottom of the vial, and the time required for 5 flies to climb above the marked line was recorded. For each experiment, at least three cohorts of 20 flies from each treatment group were scored (with three individual biological repeats for each group). Climbing latency was defined as the average time in seconds for 5 flies to climb above the marked line, with averages being pooled together from each group of 20 per treatment condition. The climbing latencies for rotenone and aripiprazole-fed flies were then normalised and expressed as a fold-change relative to that obtained for DMSO-fed flies (which was set to 1.0). For the activity assay, individual males were loaded into Drosophila Activity Monitors (DAM5) within 8×65-mm glass Pyrex tubes (Trikinetics, Waltham, MA, USA) containing fly food supplemented with 1 mM aripiprazole or 0.5% (v/v) DMSO. The flies were maintained at 25 °C under a 12-h light:12-h dark (LD) cycle. Activity data were analysed using the Sleep and Circadian Analysis MATLAB Program (SCAMP) developed by the Griffith lab [89]. The analyses were performed for 7, 14 and 21 days starting at the first ZT0 to allow acclimation. At least 16 flies of each treatment were used.

Transmission electron microscopy

For transmission electron microscopy, adult fly brains or thoraces were fixed for 2 h in 0.1 M sodium cacodylate buffer (pH 7.4) containing 2% paraformaldehyde and 2.5% glutaraldehyde (at room temperature). Then, samples were post-fixed for 1 h in a solution containing 0.25% osmium tetroxide/0.25% potassium ferrocyanide and 1% tannic acid. After fixation, the samples were stained *en bloc* with 5% aqueous uranyl acetate overnight at room temperature; then, dehydrated via a series of ethanol washes and embedded in TAAB epoxy resin (TAAB Laboratories Equipment Ltd., Aldermaston, UK). After polymerization at 65 °C for a few days, the ultrathin-sections (approximately 60 nm) obtained by Ultramicrotome (Leica Ultracut UCT, Vienna Austria) were mounted in EM grids, stained with lead citrate, and then observed by FEI Talos F200C 200 kV transmission electron microscope (Thermo Fischer Scientific, Oregon USA) with Ceta-16 M CMOS-based camera (4kx4k pixels under 16bit dynamic range). To investigate mitochondrial ultrastructural changes in flies fed DMSO, rotenone or aripiprazole, individual mitochondria were counted and ranked as either healthy, partially damaged or very damaged, and then normalised against the total number of mitochondria in that field of view. Partially damaged mitochondria were quantified as those exhibiting small areas of ultrastructural disruption, whereas very damaged mitochondria displayed areas of widespread cristae fragmentation. Images from each respective group were counted by one individual and samples blinded to eliminate the risk of sample bias.

Small-molecule conformational analyses

A selection of noncanonical complex I inhibitors including aripiprazole were flexibly aligned to the fixed conformation of complex I structure (PDB entry 7B93) using AutoDock Vina [90]. Charges were added to the ligands and receptors using AutoDockTools (https://www.ncbi.nlm.nih.gov/pmc/articles/PMC2760638). Simulations were performed at an exhaustiveness value of 300 on a high-performance computer with 64 central processing units. The top 10 binding poses were analysed, and the best conformer was selected by comparing the protein–ligand interaction energies calculated. The detailed workflow for the docking analysis, as well as the PDB coordinates of the results are available in GitHub (m1gus.github.io/Aripiprazole/).

Statistical analyses

Statistical analyses were performed using GraphPad Prism 8.0 (www.graphpad.com). The data are presented as the mean values, and the error bars indicate ± SD or SEM. In violin plots, the solid line represents the median, whereas dotted lines represent the quartiles. The number of biological replicates per experimental variable (n) is indicated in either the respective figure or figure legend. Significance is indicated as * for $p < 0.05$, ** for $p < 0.01$, *** for $p < 0.001$, and **** for $p < 0.0001$.

Supplementary Information

The online version contains supplementary material available at https://doi.org/10.1186/s13062-023-00375-9.

Additional file1. Supplementary Figures S1–S7.

Acknowledgements

We would like to thank Dr Lucia Pinon (MRC Toxicology Unit) for assistance with flow cytometry and confocal microscopy, Tim Smith and Maria Guerra Martin for help with processing of Electron Microscopy samples and Tim Ashby and Munisha Patel for preparing the fly food.

Author contributions

MMF (Lead Contact) and KRP secured funding, conceptualized and supervised the study, in collaboration with LMM. KRP, REH, LMM, JH and MMF wrote the main manuscript text with input from other authors and REH, YZY, IC and SHYL prepared figures. REH, IC, SHYL, NM, CS, MT, YZY and RS performed experiments and analysed data, with critical input from JH, KC and LP. All authors reviewed the manuscript.

Funding
This work was supported by the UK Medical Research Council (MRC), Intramural Programme Awards MC_UU_00025/4 (RG94521) to MMF and MC_UU_00025/3 (RG94521) to LMM.

Availability of data and materials
All datasets are securely archived and are available to researchers on request.

Declarations

Ethics approval and consent to participate
Not applicable.

Competing interests
The authors declare no competing interests.

Received: 1 April 2023 Accepted: 11 April 2023
Published online: 01 August 2023

References

1. McGrath J, Saha S, Chant D, Welham J. Schizophrenia: a concise overview of incidence, prevalence, and mortality. Epidemiol Rev. 2008;30:67–76.
2. Kuepper R, Skinbjerg M, Abi-Dargham A. The dopamine dysfunction in schizophrenia revisited: new insights into topography and course. Handb Exp Pharmacol. 2012;212:1–26.
3. Strange PG. Antipsychotic drugs: importance of dopamine receptors for mechanisms of therapeutic actions and side effects. Pharmacol Rev. 2001;53(1):119–33.
4. Mathews M, et al. Antipsychotic-induced movement disorders: evaluation and treatment. Psychiatry. 2005;2(3):36–41.
5. Barnes TR, McPhillips MA. Novel antipsychotics, extrapyramidal side effects and tardive dyskinesia. Int Clin Psychopharmacol. 1998;13(Suppl 3):S49-57.
6. Blair DT, Dauner A. Extrapyramidal symptoms are serious side-effects of antipsychotic and other drugs. Nurse Pract. 1992. https://doi.org/10.1097/00006205-199211000-00018.
7. Savitt D, Jankovic J. Tardive syndromes. J Neurol Sci. 2018;389:35–42.
8. Shin HW, Chung SJ. Drug-induced Parkinsonism. J Clin Neurol. 2012;8(1):15–21.
9. Casey DE. Pathophysiology of antipsychotic drug-induced movement disorders. J Clin Psychiatry. 2004;65(Suppl 9):25–8.
10. Casey DE. Tardive dyskinesia and atypical antipsychotic drugs. Schizophr Res. 1999;35(Suppl):S61-66.
11. Llorca PM, Chereau I, Bayle FJ, Lancon C. Tardive dyskinesias and antipsychotics: a review. Eu Psychiatry. 2002;17(3):129–38.
12. MEPS (2008–2018) Medical Expenditure Panel Survey (Rockville).
13. Bhattacharjee J, El-Sayeh HG. Aripiprazole versus typicals for schizophrenia. Cochr Database Syst Rev. 2008;1:Cd006617.
14. Keck PE Jr, McElroy SL. Aripiprazole: a partial dopamine D2 receptor agonist antipsychotic. Expert Opin Investig Drugs. 2003;12(4):655–62.
15. Frank A, Kiss DJ, Keseru GM, Stark H. Binding kinetics of cariprazine and aripiprazole at the dopamine D3 receptor. Sci Rep. 2018;8(1):12509.
16. Frankel JS, Schwartz TL. Brexpiprazole and cariprazine: distinguishing two new atypical antipsychotics from the original dopamine stabilizer aripiprazole. Therap Adv Psychopharmacol. 2017;7(1):29–41.
17. Azorin JM, Simon N. Dopamine receptor partial agonists for the treatment of bipolar disorder. Drugs. 2019;79(15):1657–77.
18. Bartram LA, Lozano J, Coury DL. Aripiprazole for treating irritability associated with autism spectrum disorders. Expert Opin Pharmacother. 2019;20(12):1421–7.
19. Kamijima K, Yasuda M, Yamamura K, Fukuta Y. Real-world effectiveness and safety of aripiprazole augmentation therapy in patients with major depressive disorder. Curr Med Res Opin. 2018;34(12):2105–12.
20. Robb AS, et al. Safety and tolerability of aripiprazole in the treatment of irritability associated with autistic disorder in pediatric subjects (6–17 years old):results from a pooled analysis of 2 studies. Prim Care Companion CNS Disord. 2011. https://doi.org/10.4088/PCC.10m01008gry.
21. Bernagie C, Danckaerts M, Wampers M, De Hert M. Aripiprazole and acute extrapyramidal symptoms in children and adolescents: a meta-analysis. CNS Drugs. 2016;30(9):807–18.
22. Nasrallah HA, et al. Long-term safety and tolerability of aripiprazole lauroxil in patients with schizophrenia. CNS Spectr. 2019;24(4):395–403.
23. Lungu C, et al. Tardive dyskinesia due to aripiprazole: report of 2 cases. J Clin Psychopharmacol. 2009;29(2):185–6.
24. Friedman JH. Tardive dystonia due to aripiprazole use in a neuroleptic-naive patient. J Clin Psychiatry. 2010;71(5):652–3.
25. Herrero-Mendez A, et al. The bioenergetic and antioxidant status of neurons is controlled by continuous degradation of a key glycolytic enzyme by APC/C-Cdh1. Nat Cell Biol. 2009;11(6):747–52.
26. Wu Y, Chen M, Jiang J. Mitochondrial dysfunction in neurodegenerative diseases and drug targets via apoptotic signaling. Mitochondrion. 2019;49:35–45.
27. Schapira AH, et al. Mitochondrial complex I deficiency in Parkinson's disease. Lancet. 1989;1(8649):1269.
28. Bindoff LA, Birch-Machin M, Cartlidge NE, Parker WD Jr, Turnbull DM. Mitochondrial function in Parkinson's disease. Lancet. 1989;2(8653):49.
29. Flones IH, et al. Neuronal complex I deficiency occurs throughout the Parkinson's disease brain, but is not associated with neurodegeneration or mitochondrial DNA damage. Acta Neuropathol. 2018;135(3):409–25.
30. Valente EM, et al. Hereditary early-onset Parkinson's disease caused by mutations in PINK1. Science. 2004;304(5674):1158–60.
31. Kitada T, et al. Mutations in the parkin gene cause autosomal recessive juvenile parkinsonism. Nature. 1998;392(6676):605–8.
32. Langston JW, Langston EB, Irwin I. MPTP-induced parkinsonism in human and non-human primates–clinical and experimental aspects. Acta Neurol Scand Suppl. 1984;100:49–54.
33. Zhang ZN, et al. Subcutaneous rotenone rat model of Parkinson's disease: Dose exploration study. Brain Res. 2017;1655:104–13.
34. Will Y, Dykens J. Mitochondrial toxicity assessment in industry–a decade of technology development and insight. Expert Opin Drug Metab Toxicol. 2014;10(8):1061–7.
35. Uetrecht J, Naisbitt DJ. Idiosyncratic adverse drug reactions: current concepts. Pharmacol Rev. 2013;65(2):779–808.
36. Marroquin LD, Hynes J, Dykens JA, Jamieson JD, Will Y. Circumventing the Crabtree effect: replacing media glucose with galactose increases susceptibility of HepG2 cells to mitochondrial toxicants. Toxicol Sci. 2007;97(2):539–47.
37. Kirschbaum KM, et al. Serum levels of aripiprazole and dehydroaripiprazole, clinical response and side effects. World J Biol Psychiatry. 2008;9(3):212–8.
38. Sakurama K, et al. Analysis of the binding of aripiprazole to human serum albumin: the importance of a Chloro-group in the chemical structure. ACS Omega. 2018;3(10):13790–7.
39. Sykes DA, et al. Extrapyramidal side effects of antipsychotics are linked to their association kinetics at dopamine D(2) receptors. Nat Commun. 2017;8(1):763.
40. Bolam JP, Pissadaki EK. Living on the edge with too many mouths to feed: why dopamine neurons die. Mov Disord. 2012;27(12):1478–83.
41. Donlea JM, et al. Recurrent circuitry for balancing sleep need and sleep. Neuron. 2018;97(2):378-389.e374.
42. Ueno T, et al. Identification of a dopamine pathway that regulates sleep and arousal in Drosophila. Nat Neurosci. 2012;15(11):1516–23.
43. Costa AC, Loh SH, Martins LM. Drosophila Trap1 protects against mitochondrial dysfunction in a PINK1/parkin model of Parkinson's disease. Cell Death Dis. 2013;4(1):e467.
44. Nazir A, Mukhopadhyay I, Saxena DK, Chowdhuri DK. Evaluation of the no observed adverse effect level of solvent dimethyl sulfoxide in drosophila melanogaster. Toxicol Mech Methods. 2003;13(2):147–52.
45. Miller DD, et al. Extrapyramidal side-effects of antipsychotics in a randomised trial. Br J Psychiatry. 2008;193(4):279–88.
46. Pae CU. A review of the safety and tolerability of aripiprazole. Expert Opin Drug Saf. 2009;8(3):373–86.
47. Eaves S, Rey JA. Brexpiprazole (Rexulti): a new monotherapy for schizophrenia and adjunctive therapy for major depressive disorder. Pharm Therap. 2016;41(7):418–22.
48. Nasrallah HA, et al. The safety and tolerability of cariprazine in long-term treatment of schizophrenia: a post hoc pooled analysis. BMC Psychiatry. 2017;17(1):305.

49. Cikankova T, Fisar Z, Bakhouche Y, Luptak M, Hroudova J. In vitro effects of antipsychotics on mitochondrial respiration. Naunyn-Schmiedeberg's Arch Pharmacol. 2019. https://doi.org/10.1007/s00210-019-01665-8.
50. Modica-Napolitano JS, Lagace CJ, Brennan WA, Aprille JR. Differential effects of typical and atypical neuroleptics on mitochondrial function in vitro. Arch Pharmacal Res. 2003;26(11):951–9.
51. Elmorsy E, et al. Effect of antipsychotics on mitochondrial bioenergetics of rat ovarian theca cells. Toxicol Lett. 2017;272:94–100.
52. Balijepalli S, Boyd MR, Ravindranath V. Inhibition of mitochondrial complex I by haloperidol: the role of thiol oxidation. Neuropharmacology. 1999;38(4):567–77.
53. Burkhardt C, Kelly JP, Lim YH, Filley CM, Parker WD Jr. Neuroleptic medications inhibit complex I of the electron transport chain. Ann Neurol. 1993;33(5):512–7.
54. Russell DA, et al. Hydroxylated rotenoids selectively inhibit the proliferation of prostate cancer cells. J Nat Prod. 2020;83(6):1829–45.
55. de Bartolomeis A, Tomasetti C, Iasevoli F. Update on the mechanism of action of aripiprazole: translational insights into antipsychotic strategies beyond dopamine receptor antagonism. CNS Drugs. 2015;29(9):773–99.
56. Yokoi F, et al. Dopamine D2 and D3 receptor occupancy in normal humans treated with the antipsychotic drug aripiprazole (OPC 14597): a study using positron emission tomography and [11C]raclopride. Neuropsychopharmacology. 2002;27(2):248–59.
57. Kapur S, et al. A positron emission tomography study of quetiapine in schizophrenia: a preliminary finding of an antipsychotic effect with only transiently high dopamine D2 receptor occupancy. Arch Gen Psychiatry. 2000;57(6):553–9.
58. Remington G, Kapur S. D2 and 5-HT2 receptor effects of antipsychotics: bridging basic and clinical findings using PET. J Clin Psychiatry. 1999;60(Suppl 10):15–9.
59. Kasper S, et al. Dopamine- and serotonin-receptors in schizophrenia: results of imaging-studies and implications for pharmacotherapy in schizophrenia. Eur Arch Psychiatry Clin Neurosci. 1999;249(Suppl 4):83–9.
60. Ishigooka J, Iwashita S, Higashi K, Liew EL, Tadori Y. Pharmacokinetics and safety of Brexpiprazole following multiple-dose administration to Japanese patients with schizophrenia. J Clin Pharmacol. 2018;58(1):74–80.
61. Nakamura T, et al. Clinical pharmacology study of cariprazine (MP-214) in patients with schizophrenia (12-week treatment). Drug Des Devel Ther. 2016;10:327–38.
62. Mallikaarjun S, Salazar DE, Bramer SL. Pharmacokinetics, tolerability, and safety of aripiprazole following multiple oral dosing in normal healthy volunteers. J Clin Pharmacol. 2004;44(2):179–87.
63. Kirschbaum KM, et al. Pharmacokinetics of acute and sub-chronic aripiprazole in P-glycoprotein deficient mice. Neuropharmacology. 2010;59(6):474–9.
64. Kornhuber J, et al. Persistence of haloperidol in human brain tissue. Am J Psychiatry. 1999;156(6):885–90.
65. Wang JS, et al. Aripiprazole brain concentration is altered in P-glycoprotein deficient mice. Schizophr Res. 2009;110(1–3):90–4.
66. De Vries MC, et al. Safety of drug use in patients with a primary mitochondrial disease: an international Delphi-based consensus. J Inherit Metab Dis. 2020;43(4):800–18.
67. Gaweda-Walerych K, et al. Mitochondrial DNA haplogroups and subhaplogroups are associated with Parkinson's disease risk in a Polish PD cohort. J Neural Transm. 2008;115(11):1521–6.
68. Kenney MC, et al. (2014) Molecular and bioenergetic differences between cells with African versus European inherited mitochondrial DNA haplogroups: implications for population susceptibility to diseases. Biochim Biophys Acta. 1842;2:208–19.
69. Stewart JB, Chinnery PF. Extreme heterogeneity of human mitochondrial DNA from organelles to populations. Nat Rev Genet. 2021;22(2):106–18.
70. Jones SW, Ball AL, Chadwick AE, Alfirevic A. The role of mitochondrial DNA variation in drug response: a systematic review. Front Genet. 2021;12:698825.
71. Chung I, et al. Cork-in-bottle mechanism of inhibitor binding to mammalian complex I. Sci Adv. 2021;7(20):eabg4000.
72. Stephenson ZA, et al. Identification of a novel toxicophore in anti-cancer chemotherapeutics that targets mitochondrial respiratory complex I. Elife. 2020;9:e55845.
73. Grba DN, Hirst J. Mitochondrial complex I structure reveals ordered water molecules for catalysis and proton translocation. Nat Struct Mol Biol. 2020;27(10):892–900.
74. Kampjut D, Sazanov LA. The coupling mechanism of mammalian respiratory complex I. Science. 2020;370:eabc4209.
75. Hirose T, et al. Mechanism of action of aripiprazole predicts clinical efficacy and a favourable side-effect profile. J Psychopharmacol. 2004;18(3):375–83.
76. Pruszak J, Just L, Isacson O, Nikkhah G. Isolation and culture of ventral mesencephalic precursor cells and dopaminergic neurons from rodent brains. Curr Protoc Stem Cell Biol. 2009. https://doi.org/10.1002/9780470151808.sc02d05s11.
77. Currle DS, Hu JS, Kolski-Andreaco A, Monuki ES. Culture of mouse neural stem cell precursors. J Vis Exp. 2007;2:152.
78. (2012) Dissection and Culture of Mouse Dopaminergic and Striatal Explants in Three-Dimensional Collagen Matrix Assays Journal of Visualized Experiments (61) 10.3791/3691
79. Robinson GL, Dinsdale D, Macfarlane M, Cain K. Switching from aerobic glycolysis to oxidative phosphorylation modulates the sensitivity of mantle cell lymphoma cells to TRAIL. Oncogene. 2012;31(48):4996–5006.
80. Salabei JK, Gibb AA, Hill BG. Comprehensive measurement of respiratory activity in permeabilized cells using extracellular flux analysis. Nat Protoc. 2014;9(2):421–38.
81. Agip AA, Blaza JN, Fedor JG, Hirst J. Mammalian respiratory complex I through the lens of Cryo-EM. Annu Rev Biophys. 2019;48:165–84.
82. Blaza JN, Serreli R, Jones AJ, Mohammed K, Hirst J. Kinetic evidence against partitioning of the ubiquinone pool and the catalytic relevance of respiratory-chain supercomplexes. Proc Natl Acad Sci USA. 2014;111(44):15735–40.
83. Jones AJ, Hirst J. A spectrophotometric coupled enzyme assay to measure the activity of succinate dehydrogenase. Anal Biochem. 2013;442(1):19–23.
84. Jones AJ, et al. A self-assembled respiratory chain that catalyzes NADH oxidation by ubiquinone-10 cycling between complex I and the alternative oxidase. Angew Chem Int Ed Engl. 2016;55(2):728–31.
85. Biner O, Fedor JG, Yin Z, Hirst J. Bottom-up construction of a minimal system for cellular respiration and energy regeneration. ACS Synth Biol. 2020;9(6):1450–9.
86. Bason JV, Runswick MJ, Fearnley IM, Walker JE. Binding of the inhibitor protein IF(1) to bovine F(1)-ATPase. J Mol Biol. 2011;406(3):443–53.
87. Powley IR, Hughes MA, Cain K, MacFarlane M. Caspase-8 tyrosine-380 phosphorylation inhibits CD95 DISC function by preventing procaspase-8 maturation and cycling within the complex. Oncogene. 2016;35(43):5629–40.
88. Kohlhaas SL, Craxton A, Sun XM, Pinkoski MJ, Cohen GM. Receptor-mediated endocytosis is not required for tumor necrosis factor-related apoptosis-inducing ligand (TRAIL)-induced apoptosis. J Biol Chem. 2007;282(17):12831–41.
89. Donelson NC, et al. High-resolution positional tracking for long-term analysis of Drosophila sleep and locomotion using the "tracker" program. PLoS ONE. 2012;7(5):e37250.
90. Trott O, Olson AJ. AutoDock Vina: improving the speed and accuracy of docking with a new scoring function, efficient optimization, and multithreading. J Comput Chem. 2010;31(2):455–61.

Publisher's Note